Augmented Temperature Degrading Effect of Rare Earth Magnets Arranged in Segmented Halbach Arrays

Oliver Winter[1], Christian Kral[1], and Erich Schmidt[2]

[1]AIT Austrian Institute of Technology, Mobility Department, Electric Drive Technologies, 1210 Vienna, Austria
[2]Vienna University of Technology, Institute of Energy Systems and Electrical Drives, 1040 Vienna, Austria

If rare earth magnets are arranged in a Halbach array, flux concentration occurs at one side of the array. This principle can be utilized in electric machines to augment the air-gap flux density or even to omit flux carrying iron parts. Highly utilized electric machines are operated at elevated temperatures requiring an appropriate selection of the material. However, the uncommon magnet orientation required in a Halbach array entails an augmented temperature degrading effect in the magnets. The effect is studied in three test cases with linear arrangements of Halbach arrays by means of 2-D and 3-D Finite Element Analysis and is validated through measurements.

***Index Terms*—Demagnetization, finite element methods, permanent magnets, rare earth metals, temperature degrading.**

I. Introduction

A multitude of electrical machines and drive concepts were developed cater for the global demand on advanced electric vehicles. One of the most lightweight and efficient topologies was presented in [1]. This axial flux design with air cored stator winding is excited by two outer magnet rings. The application of Halbach arrays in lieu of iron back rings was proposed by [1], but today only the conventional design is commercially available. The effect of magnetic flux concentration caused by an alternating magnetization pattern was discovered by Mallinson [2] in 1973 who worked in the field of magnetic recording techniques. The physicist K. Halbach found another practical application for this effect: synchrotron undulators and multipoles [3]. Since then, usually radial flux machines [4] were equipped with Halbach arrays but it is shown that air cored axial flux machines are the better choices, in particular if efficiency and weight are important [5]. In the current paper, we adopt the suggestion of using Halbach arrays in an air cored axial flux motor to reach both highest possible efficiency and minimum added mass.

The nexus between the temperature and torque production using rare earth magnets has already been discussed in [6]. Moreover, the use of Halbach arrays in synchronous machines has been analyzed in [7]. The combination of both topics and their influence on torque production under real operational conditions is of great interest for our ongoing research project, where we will first focus on a prototype machine. The essential objective of this paper is the analysis of the temperature dependent behavior of Halbach arrays. The flux distribution within the magnets and in the air-gap is analyzed in detail by means of Finite Element Analysis (FEA). An example of the resulting magnetization pattern and the magnetic flux line distribution is shown in Fig. 1(i) and (ii), respectively.

Manuscript received March 02, 2012; revised April 23, 2012; accepted May 10, 2012. Date of current version October 19, 2012. Corresponding author: O. Winter (e-mail: oliver.winter@ait.ac.at).

Digital Object Identifier 10.1109/TMAG.2012.2199850

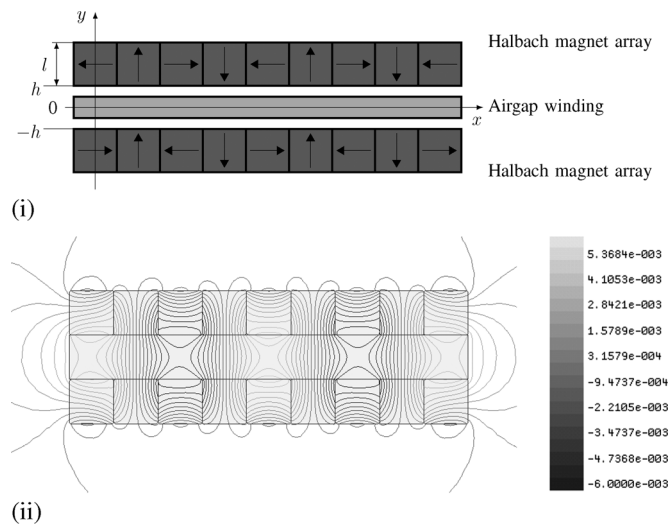

Fig. 1. Double sided Halbach magnet array arrangement without back iron, (i) magnetization pattern, (ii) magnetic flux lines.

II. Analytical Model of the Air-Gap Field

Considering a wide planar structure with respect to a Cartesian coordinate system as indicated in Fig. 1(i), the magnetic flux density and the magnetic vector potential $\mathbf{A}$ fulfils

$$\mathbf{B} = \nabla \times \mathbf{A} \quad \text{and} \quad \Delta \mathbf{A} = \mathbf{0}. \tag{1}$$

With respect to the period length λ we have $\mathbf{A}(x+\lambda) = \mathbf{A}(x)$. Applying the method of separation of variables with $k = 2\pi/\lambda$, the tangential and normal component of the magnetic flux density are

$$B_x(x,y) = \sum_{n=1}^{\infty} B_{y0n} \cos(nkx) \frac{\sinh(nky)}{\cosh(nkh)} \tag{2a}$$

$$B_y(x,y) = \sum_{n=1}^{\infty} B_{y0n} \sin(nkx) \frac{\cosh(nky)}{\cosh(nkh)} \tag{2b}$$

where a boundary condition

$$B_y(x,h) = B_{y0} = \sum_{n=1}^{\infty} B_{y0n} \sin(nkx) \tag{3}$$

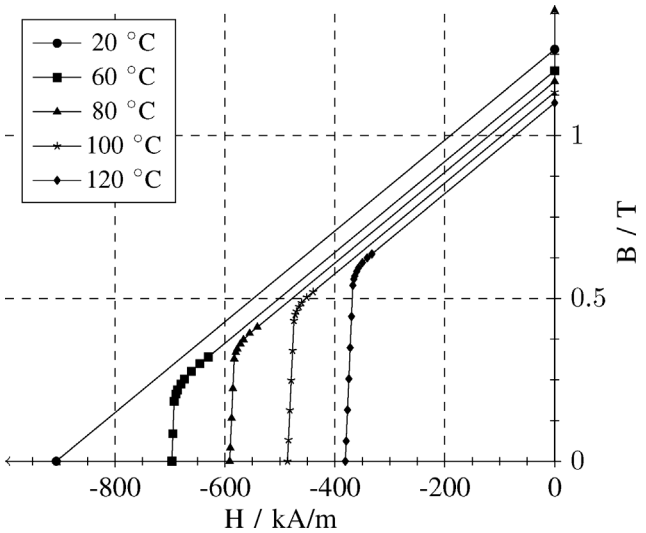

Fig. 2. Typical second quadrant demagnetization data, material grade N40, maximum operation temperature 80°C.

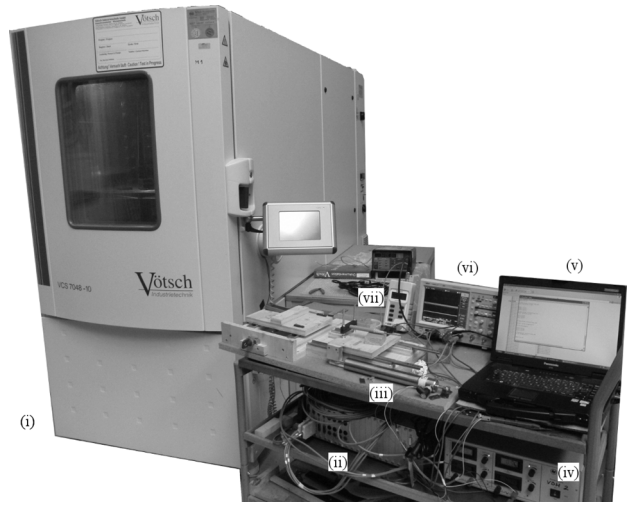

Fig. 3. Measurement setup, (i) climate cabinet, (ii) Cronos PL measurement system with temperature and voltage input channels, (iii) linear position sensor attached to the test carriage, (iv) DC supply, (v) notebook, (vi) digital oscilloscope, (vii) Gauss meter with axial hall probe attached to the test carriage.

at the magnet surface is assumed. An alternative approach originally published by Mallinson [2] is described in [8]. There, the magnetization pattern is approximated by the superposition of two sinusoids in quadrature, i.e.,

$$M_x = M_0 \sin(kx), \quad M_y = M_0 \cos(kx), \quad M_z = 0. \tag{4}$$

M_0 is the magnetization magnitude. This formulation includes only the fundamental harmonic. The potential inside the magnet array satisfies Poisson's equation and yields the resulting peak value

$$\hat{B} = B_r(1 - \mathrm{e}^{-kl})\mathrm{si}\left(\frac{\pi}{n_m}\right). \tag{5}$$

at the surface. Here, B_r denotes the remanent flux density, l is the magnet height and n_m is the number of magnet blocks per period [9]. However, the magnetization pattern shown in Fig. 1(i) is not adequately captured by (4). In order to include the higher harmonics and the finite length of the Halbach array, FEA is applied in the following.

III. Material Definition and Detailed Finite Element Analyses

The temperature-dependent decrease of the coercive field strength and the remanent flux density is usually modeled by linear or second-order characteristics. In this paper, a linear temperature dependency of the characteristic magnetic properties is considered. In standard applications, magnets are usually used in easy axis directions. In 90° Halbach arrays, only in the gap magnets, i.e. those with horizontal flux lines in Fig. 1(ii), carry the flux along the easy axis direction. However, the flux in the pole magnets (vertical flux lines) mainly crosses the lateral boundaries of the magnet block. This leads to a unbalanced flux density distribution within the magnet block itself. We study this effect using both 2-D and 3-D FEA. Our analysis is based on typical manufacture's data such as nonlinear, temperature-dependent demagnetization characteristics shown in Fig. 2. The magnet material is modelled with an

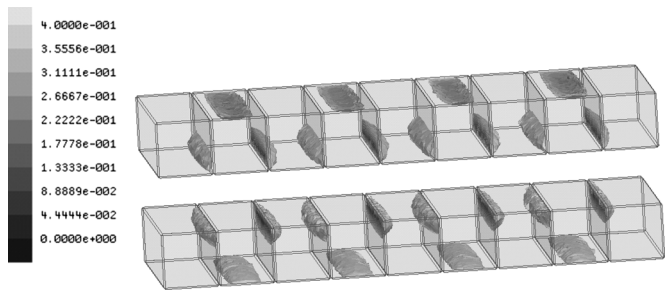

Fig. 4. Three-dimensional FEA result, magnetic flux density magnitude plot form 0 to 0.4 T to indicate the demagnetized regions within the specimen, the magnetization pattern is shown in Fig. 1(i), pole magnets are affected on the outer side and the gap magnets at the inner side corners, material grade N40, operation temperature 80°C.

isotropic relative permeabilty. In order to verify these characteristic curves, the magnetic flux density between two magnets arranged along their easy axis direction was measured for different temperatures. The setup consists of an axial Hall probe and a climate cabinet, as shown in Fig. 3. It was found that the measured air-gap flux density degrades due to temperature rise by $-0.13\%/°\mathrm{C}$. This value is in reasonable accordance with the value reported in the literature value ($-0.12\%/°\mathrm{C}$ for grade N40, [10]). If the load line for a given magnetic circuit intersects the relevant characteristic curve in Fig. 2 above its the knee, only reversible demagnetization takes place. This is the desired standard case. In Halbach array magnets however, local flux concentrations may cause local irreversible demagnetization already at the maximum operational temperature or even below. Explaining and analyzing this undesirable demagnetization effect of Halbach arrays is the main contribution of the current paper. To illustrate the effect, the 3-D magnetic flux density plot is shown in Fig. 4 for the range 0 to 0.4 T (lowest value of the linear characteristic for 80 °C for N40 material, cf. Fig. 2). The underlying magnetostatic FEA model consists of approximately 170000 second-order tetrahedral elements. In Fig. 4, 3% of the total magnet volume is affected

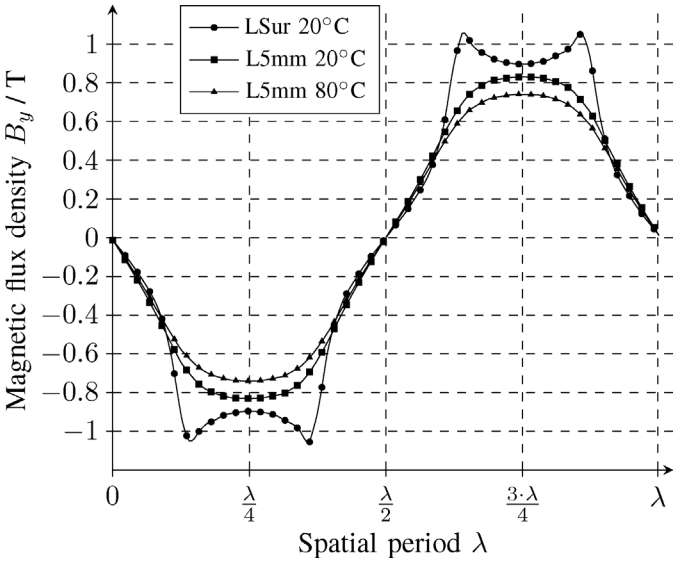

Fig. 5. Two-dimensional FEA result, double sided Halbach array, flux density B_y for two different operation temperatures (20 °C and 80 °C) at 5 mm distance and 20 °C at the surface), air-gap 10 mm, N40 magnet material.

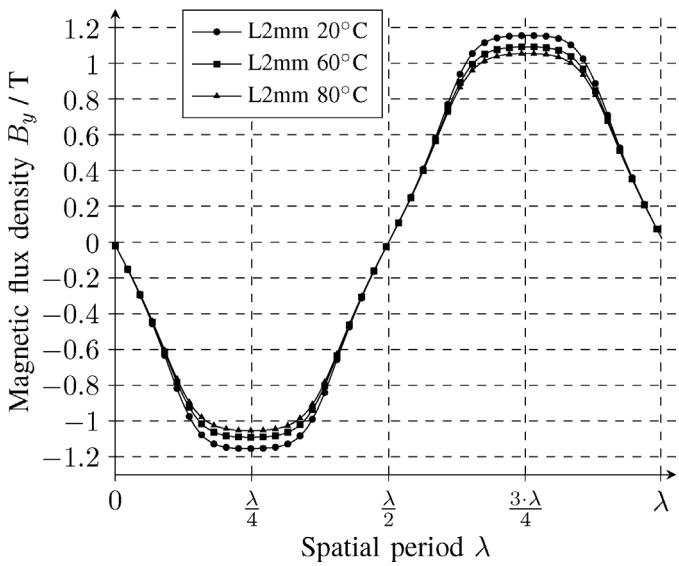

Fig. 6. Two-dimensional FEA result, double sided Halbach array, flux density B_y for different operation temperatures (20 °C, 60 °C, and 80 °C) at 2 mm distance and 20 °C at the surface), air-gap 5 mm, N40 magnet material.

by local irreversible demagnetization at 80 °C. These volumes are located at the pole magnet outer side and at the gap magnets inner side corners. Even if the operating temperature decreases, the affected volumes remain demagnetized. To study the impact of the described augmented temperature degrading phenomenon on the operation of linear electric machines, three test cases were modeled with FEA (N40 double array with air-gap $\delta = 5$ mm, N40 double array with air-gap $\delta = 10$ mm, N35 single array). The normal flux density component B_y on the surface of the array is shown Fig. 5. This cleary shows that neither the assumption of sinusoidal boundary condition (3) nor the first harmonic approach (4) is tenable. Hence, FEA is our preferred analysis tool. The magnetic flux density was evaluated at 2 mm and 5 mm distance, denoted by L2 mm and

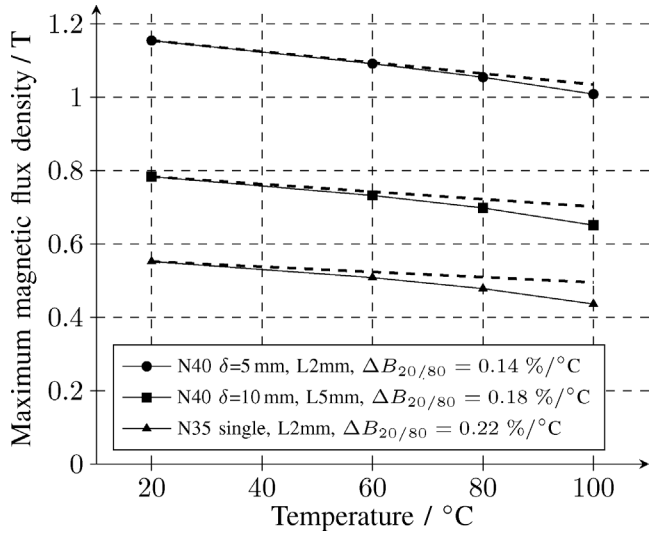

Fig. 7. Two-dimensional FEA result for three different 9 pieces Halbach arrangements and materials, (N40 double with air-gap 5 mm, N40 double with air-gap 10 mm, N35 single), Lymm represents the evaluation distance, dashed line indicates $-0.13\%/°$C theoretical decrease, $\Delta B_{20/80}$ is the linear interpolated slope from 20 °C to 80 °C.

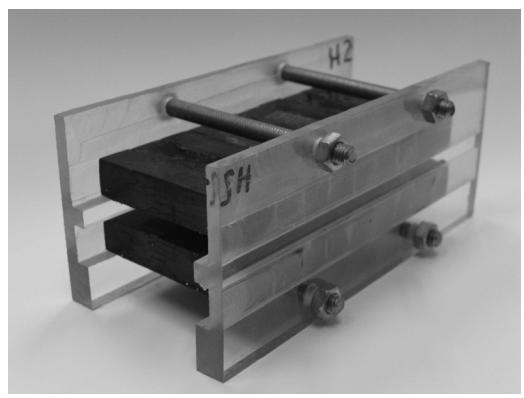

Fig. 8. Functional model, double sided N40 Halbach magnet arrays (2 × 9 pieces 10 × 10 × 45 mm each), air-gap $\delta = 5$ mm.

L5 mm respectively.As shown in Fig. 5, the spatial distribution at L5 mm is not affected by the temperature difference. The same assumptions holds for L2 mm (cf. Fig. 6). Therefore, the maximum value was used to compare different operating temperatures. The results for the three test cases are shown in Fig. 7. While the literature and our measurements using on the two magnet configuration predict the remanence flux density reduces by 0.13%/°C (dashed line in Fig. 7), the FEA result shows that the degrading is significantly increased in Halbach arrays, especially with increased air-gaps.

IV. Experimental Validation

The three test scenarios described in the previous section have been verified in an experimental analysis. The N40 double array with an air-gap of $\delta = 5$ mm is shown in Fig. 8. The respective test specimen was placed in a climate cabinet to establish various operating temperatures. The overall test setup is shown in Fig. 3. After reaching the thermal equilibrium, the Halbach array was placed on the measurement device. The configuration

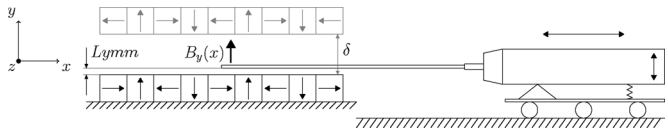

Fig. 9. Measurement principle, axial hall probe attached to the test carriage.

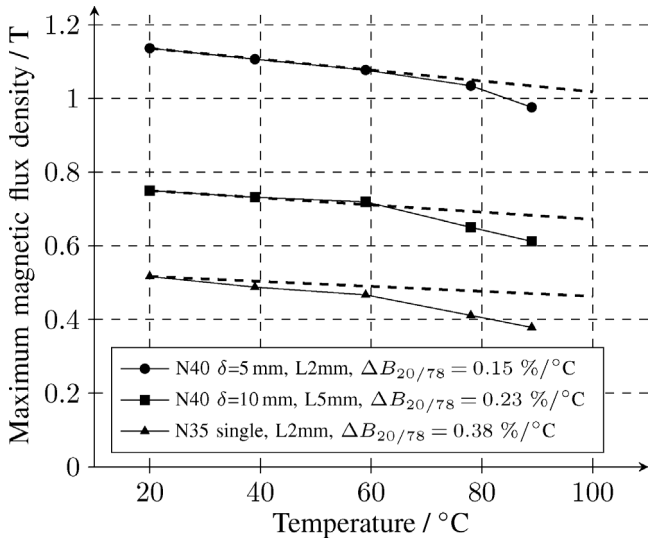

Fig. 10. Measurement result for three different Halbach arrangements (consisting of 9 magnet pieces) and materials, (N40 double with air-gap 5 mm, N40 double with air-gap 10 mm, N35 single), Lymm represents the evaluation distance, dashed line indicates $-0.13\%/°$C theorectical decrease, $\Delta B_{20/78}$ is the linear interpolated slope from 20 °C to 78 °C.

is shown in Fig. 9. The axial Hall sensor is attached to a test carriage traveling along the direction x. While moving said carriage, the flux density measured by the Hall sensor was recorded together with the respective position. Various calibrated PT100 thermocouples for monitoring the ambient temperature, the climate chamber air temperature and the magnet array temperature of an additional array which remained inside the chamber. The Hall sensor temperature rise due to heat radiation during the measurement period of around 10 s per sample is negligible. Representative measurements result are shown in Fig. 10. The value Lymm describes again the perpendicular distance between the inner magnet surface and the probe. It is assumed, that the difference between the measurements and the FEA is caused by uncertain magnet material parameters (e.g. different permeability characteristics along and perpendicular to the easy axis) and the adhesive gap between the magnets.

V. Conclusion

This paper discusses the effect of augmented temperature degrading of rare earth magnets arranged in 90° Halbach arrays. Both 2-D and 3-D nonlinear magnetostatic FEA provided new insights into the effect of local demagnetization in Halbach arrays. Moreover, three different Halbach magnet arrangements with N35 and N40 magnet material were fabricated. A Hall probe was moved through the functional models at various magnet temperatures. In this way, the magnetic flux density distribution was measured. Both numerical analyses as well as measurements confirm the occurrence of the augmented temperature degrading effect.

Acknowledgment

The authors would like to thank the Austrian Research Promotion Agency (Oesterreichische Forschungsfoerderungsgesellschaft mbH, Klima- und Energiefonds, Neue Energien 2020) for the research project 829727 *HeAL—High efficient ironless drive for lightweight vehicles*.

References

[1] H. Lovatt, V. Ramsden, and B. Mecrow, "Design of an in-wheel motor for a solar-powered electric vehicle," *IEE Proc. Elect. Power Appl.*, vol. 145, no. 5, pp. 402–408, Sep. 1998.

[2] J. Mallinson, "One-sided fluxes—A magnetic curiosity?," *IEEE Trans. Magn.*, vol. 9, no. 4, pp. 678–682, Dec. 1973.

[3] K. Halbach, "Design of permanent multipole magnets with oriented rare earth cobalt material," *Nucl. Instrum. Meth.*, vol. 169, no. 1, pp. 1–10, 1980.

[4] Z. Zhu, Z. Xia, Y. Shi, D. Howe, A. Pride, and X. Chen, "Performance of halbach magnetized brushless ac motors," *IEEE Trans. Magn.*, vol. 39, no. 5, pp. 2992–2994, Sep. 2003.

[5] J. F. Gieras, R.-J. Wang, and M. J. Kamper, *Axial Flux Permanent Magnet Brushless Machines*, 1st ed. Dordrecht, The Netherlands: Kluwer Academic, 2004.

[6] T. Sebastian, "Temperature effects on torque production and efficiency of pm motors using ndfeb magnets," in *Proc. Conf. Rec. IEEE Industry Applications Soc. Annu. Meet.*, Oct. 1993, pp. 78–83.

[7] D. Trumper, M. Williams, and T. Nguyen, "Magnet arrays for synchronous machines," in *Proc. Conf. Rec. IEEE Industry Applications Soc. Annu. Meet.*, Oct. 1993, pp. 9–18.

[8] H. Shute, J. Mallinson, D. Wilton, and D. Mapps, "One-sided fluxes in planar, cylindrical, and spherical magnetized structures," *IEEE Trans. Magn.*, vol. 36, no. 2, pp. 440–451, Mar. 2000.

[9] K. Halbach, "Physical and optical properties of rare earth cobalt magnets," *Nucl. Instrum. Meth. Phys. Res.*, vol. 187, no. 1, pp. 109–117, 1981.

[10] M. Thompson, "Practical issues in the use of ndfeb permanent magnets in maglev, motors, bearings, and eddy current brakes," *Proc. IEEE*, vol. 97, no. 11, pp. 1758–1767, Nov. 2009, (invited).